Available online at www.sciencedirect.com
ScienceDirect
Journal of Nuclear Materials 362 (2007) 259–267
journal of nuclear materials
www.elsevier.com/locate/jnucmat

Microstructural analysis of candidate steels pre-selected for new advanced reactor systems

A. Zeman [a,*], L. Debarberis [a], J. Kočík [b], V. Slugeň [c], E. Keilová [b]

[a] Institute for Energy, Joint Research Centre of the European Commission, P.O. Box 2, 1755ZG Petten, The Netherlands
[b] Nuclear Research Institute Řež plc., Husinec – Řež 130, 250 68 Řež, Czech Republic
[c] Department of Nuclear Physics and Technology, Slovak University of Technology, Ilkovičova 3, 81219 Bratislava, Slovakia

Abstract

Many of candidate materials for Generation IV concept have been developed in past, however they have not been tested yet for new conditions and therefore, a huge effort must be carried out for their characterization and validation in the R&D phase. Moreover, the issue concerning the structural integrity of materials is going to have a more and more dominant role due to the degradation mechanisms, as hardening, thermal fatigue, creep, swelling, phase instability and embrittlement, which must be understood in order to estimate the component lifetime. This paper presents some interesting results on few candidate materials selected for Generation IV reactor concepts. The study is based on application of non-destructive spectroscopic techniques to investigate materials as EUROFER'97, P91 and T91.

PACS: 61.80.−x; 61.72.Ji; 81.05.−t; 81.40.Wx; 61.80.Jh; 68.37.Lp

1. Introduction

The new sources of energy based on nuclear technologies are under development at the moment. Several studies have confirmed that the development of new energy sources, which do not emit greenhouse gases (GEG), is a promising way to solve the problem of energy production and decrease the GEG emission. Nowadays, the different nuclear reactor concepts are studied in the international forum called, 'Generation IV'. The six concepts are already selected for future installations, in particular gas-cooled fast reactor (GFR), lead-cooled fast reactor (LFR), molten salt reactor (MSR), sodium-cooled fast reactor (SFR), supercritical water-cooled reactor (SCWR) and very-high-temperature reactor (VHTR). Some of them seem to be very effective from the sustainability point of view.

The main role of new NPPs covered by the Generation IV concept is to provide sustainable energy generation that meets clean air objectives and promotes long-term availability of systems and effective fuel utilization for worldwide energy production. However, one of the most important pre-requisities for this new types of nuclear installations, is the highest possible level of safety, effective economics and finally, enhanced proliferation resistance. In view of

* Corresponding author. Tel.: +31 224 565467; fax: +31 224 565636.
E-mail address: Andrej.Zeman@jrc.nl (A. Zeman).

0022-3115/$ - see front matter © 2007 Elsevier B.V. All rights reserved.
doi:10.1016/j.jnucmat.2007.01.068

these requirements the material aspects for components becomes, therefore very important. It is also important to minimize and manage their nuclear waste and notably reduce the long-term stewardship burden, thereby improving protection for the public health and the environment. Proliferation resistance and physical protection will ensure that they are a very unattractive and the least desirable route for diversion or theft of weapons-usable materials, and minimize their vulnerability. The R&D phase will be guided by the technology/material roadmap developed for the Generation IV International Forum (GIF) over several years with the participation of several partners from the GIF countries.

The phenomenon, the so-called radiation embrittlement, is the most important, with regard to practice, consequence of neutron irradiation on reactor pressure vessel (RPV) and internals steels behaviour. The degradation of RPV steel is a very complicated process dependent on many factors (thermal treatments and radiation exposure, chemical compositions, fabrication and post-production processing conditions, etc.). This topic has been the subject of many comprehensive works [1,2]. However, the related neutron embrittlement and microstructural changes remain only partially understood. The effect of intensive fluxes of neutrons results in considerable changes of material structures and properties. In particular, the development of fine scale radiation-induced defects which impede the dislocation motion under applied stress, known as irradiation embrittlement, leads to mechanical properties degradation which can result in partial loss of plasticity and in an increase incidence of brittle fracture [3]. Defects are formed from vacancies and interstitials created in collision cascaded processes. Those point defects surviving the cascades migrate freely through the crystal lattice, interacting with each other and with solute atoms in the matrix and also with dislocation substructure and precipitates. These irradiation-induced diffusion processes result in the formation of new point defect clusters, dislocation loops and precipitates [4]. The irradiation embrittlement and hardening phenomenon should also be a serious issue for the new types of reactors, called Generation IV. Therefore, a wide-range of testing has to be performed during R&D phase of new steels for RPVs and internals.

Since 1980s, several improved ferritic–martensitic (FM) steels have been developed for the power-generation industry. For these newer steels, no complete irradiation data exist, although it would not be expected that these steels will behave differently from steels for which more extensive data are available (HT9, EM12, FV448, etc.). It is anticipated that further developments with variations in the modified 9Cr–1Mo class of ferritic–martensitic steels will provide a material with superior high-temperature creep strength than currently available and with far superior radiation resistance than 2 1/4Cr–1Mo steel. In the case of new reactor systems (GCR, SWCR, LFR), the research and development program should incorporate more advanced materials in the overall class of ferritic–martensitic steels, some of which are currently in R&D phase.

This work is oriented mainly to the evaluation of microstructural properties of some pre-selected ferritic–martensitic steels, in particular hardening and lattice defects incubation due to irradiation. The new advanced types of steels have to be widely tested before their final implementation. The potentially interested materials for application in Generation IV concepts are FM steels, such as P91 and T91 [5], and possibly advanced FM steels with reduced-activation (RAFM), as EUROFER'97. Besides the standard mechanical testing the application of additional methods is essential for better understanding such kind of mechanism at microstructural level. The benefits of non-destructive methods, as positron annihilation spectroscopy (PAS) potentially combined with transmission electron microscopy (TEM) can be very helpful and appropriate in this, as it has been confirmed by recently published data [6]. Understanding of radiation effects in FM/RAFM alloys is a critical milestone for their future application in new reactor systems.

2. Experiment: techniques, materials and treatments

2.1. Techniques

This experimental research is coordinated by the Institute of Energy, Joint Research Center (JRC-IE) of European Commission in Petten and involves also Nuclear Research Institute Rez (NRI) and the Slovak University of Technology Bratislava (STU). The main part of the experimental testing was done in the testing laboratories of JRC (positron annihilation spectroscopy and hardness measurements). The other partners have contributed to the part of irradiation experiments (1 MeV cascade accelerator) and application of microscopy investigation, light optical microscopy (LOM) and transmission electron

microscopy (TEM). Generally, this common initiative is performed within the frame of SAFELIFE action of JRC-IE Petten.

Positron annihilation spectroscopy (PAS) is applied to study the electronic and atomic structure of materials. The standard lifetime fast-fast setup was used with the resolution FWHM 250 ps. The positron source (~2.5 MBq of ^{22}Na encapsulated into a kapton foil of 7.5 μm thickness) was sandwiched between two identical samples ($10 \times 10 \times 0.4$ mm, 1 μm one-face polished) of the investigated steel. At least 5 million counts have been collected per spectra; thereafter spectra were evaluated by LT9 software. The PAS technique is especially sensitive to open volume defects like vacancies and their clusters [7]. In solids, positrons reside mainly in the interstitial region because the repulsion of nuclei is weak here [8]. In open volume defects this repulsion is even weaker and positrons can get trapped in such defects because they constitute a potential for positrons. Irradiation damage is the usual way of production of vacancies and their agglomerates that are typical examples of open volume defects [9].

Transmission electron microscopy (TEM) examinations were conducted with JEOL 2010, operated at 200 keV. Thin foils were prepared by mechanical grinding to the thickness of ~80 μm and by double jet polishing in 7% perchloric acid, methanol, at −225 K and ~22 V. TEM is an essential tool to understand the microstructural features of this and similar type of alloys. TEM enables to study the lath and sub-grain dimensions, dislocation densities, carbide dimensions, carbide compositions, and carbide population statistics, all of which evolve with aging.

Hardness Vickers measurements (HV) were carried-out both prior to and after irradiation by protons. The measurements were done using a Shimadzu HSV-20 instrument. Indents were made on a PAS samples in both the irradiated state and the unirradiated state. The proton irradiation produces a fairly uniform damage region over approximately the 1.5 μm.

2.2. Ferritic–martensitic steels

Reference test materials from different manufacturers have been collected and tested. The ferritic–martensitic steels P91 and T91 with the composition 9Cr–1Mo and minor alloying elements Ni, Nb, V, and C were selected. On the other hand, the key representative of RAFM steels, the EUROFER'97 has been selected as reference material. The high temperature strength and radiation stability of this alloy, makes it an attractive candidate for applications in reactor and spallation environments. FM steels are attractive because of their resistance to radiation-induced swelling. The chemical composition of selected FM steels is given in Table 1. The alloys were used in the normalized and tempered condition, as noted in Table 1.

EUROFER'97 is the reference 9CrWVTa steel for the European long-term fusion programme. It is envisaged as a structural steel for the tritium-breeding blanket in a DEMO type plant, and for blanket mock-ups in ITER. It combines moderately high service temperature (<825 K), good post-irradiation toughness and transition temperature and has shown post-irradiation chemical and dimensional stability [10].

P91 was developed in the 1970s as part of a program for developing advanced creep resistant alloys for fast breeder power reactor programs. The drive for increasing thermal efficiency in fossil fuelled power plant has resulted in the introduction of supercritical pressure systems for delivering steam at temperatures of 875 K. Conventional low alloy

Table 1
Chemical composition of alloying elements and impurities (wt%) of selected ferritic–martensitic steels

Element/steel (manufacturer)	EUROFER'97[a] (Böhler)	P91[b] (Mannesmann)	T91[c] (Industeel)
C	0.11	0.106	0.1025
Si	0.04	0.32	0.22
Mn	0.48	0.47	0.38
Cr	8.82	8.93	8.99
Ni	0.02	0.3	0.11
Cu	0.0016	0.11	0.06
S	0.004	0.001	0.0004
P	0.005	0.016	0.021
V	0.20	0.21	0.21
Mo	<0.001	0.94	0.89
N	0.02	0.065	0.0442
Al	0.009	0.012	–
Co	0.006	–	–
Ta	0.13	–	–
O	0.001	–	–
Nb	0.0016	0.067	0.06
W	1.08	–	0.01
Ti	0.006	0.003	0.0034
Sn	<0.005	–	0.004
Hardness Vickers (–)	192	208	224

Heat treatment (normalisation/tempering): [a]1255 K/27 min air/1035 K/1.5 h air, [b]1335 K/1.1 h air/1035 K/2.2 h air, [c]1325 K/15 min air/1035 K/45 min air.

steels such 2.25Cr–1Mo have unacceptable creep performance at these temperatures, hence more highly alloyed steels are required, like modified 9Cr–1Mo martensitic alloy, with enhanced creep properties provided by micro-alloying additions of Nb, V and N. Fine scale Nb and V carbonitride/nitrides can interact with dislocations and provide strengthening, while larger scale $Cr_{23}C_6$ precipitation on lath, grain and sub-grain boundaries provides pinning, thus stabilizing the microstructure [11].

T91 has been developed in the US fusion materials program on modified 9Cr–1Mo, as a second-generation steel. The T91 showed significantly improved irradiation resistance compared to that of HT9, primarily because of the lower carbon concentration. In particular, under irradiation conditions where HT9 develops an increase in the ductile-brittle transition temperature of 395–425 K, the modified 9Cr–1Mo developed a shift of only 325–327 K. For the very high neutron exposures anticipated for some LFR components, the reduced radiation sensitivity may be critical [12].

2.3. Light optical microscopy

The micrographs (Fig. 1) show typical microstructures of all steels as observed by light optical microscopy (LOM). Whereas the microstructures of P91 and T91 steels are typical for tempered martensites, the EUROFER'97 microstructure resembles most likely the morphology of ferritic/carbidic mixtures. In addition, few coarse inclusions have been also found by lightoptical microscopy in EUROFER'97 steel. The prior austenite grain size is smaller in the EUROFER'97 steel containing Ta and being normalized at lower temperature (1255 K) in comparison to P91 and T91 steels. Both 9Cr1MoVNb type steels, normalized at 345 and 355 K higher temperatures, posses coarser prior austenite grain size.

2.4. Proton irradiation

The objective of the proton irradiation of FM steels is to evaluate the microstructural changes due to radiation hardening and embrittlement phenomenon. Irradiations were conducted with 500 keV H_2 to doses of 0.7, 2 and 3.5 displacement-per-atom (dpa) at temperatures of 395 K. The sample temperature was maintained within ± 10 K during the whole irradiation process. Samples were treated by proton (p) bombardment with the aim to simulate the radiation damage and embrittlement, which is induced by neutrons in real RPV materials. The dpa dose was derived and calculated by SRIM code [13] in order to characterise the radiation damage.

Proton irradiation has been proven as effective tool in emulating the effects of neutron irradiation in austenitic stainless steel used in light water reactor cores. Radiation-induced segregation, dislocation microstructure, irradiation hardening, void formation and susceptibility to irradiation assisted stress corrosion cracking are example mechanisms that have been shown to be emulated by proton irradiation [10]. This investigation will serve to generate the data on irradiation effects on ferritic–martensitic steels P91, T91 and EUROFER'97 in an effort to learn how this alloy responds to irradiation and how the microstructure develops with dose and temperature.

Different prediction models can be applied in case PWR reactor pressure vessel (RPV). However

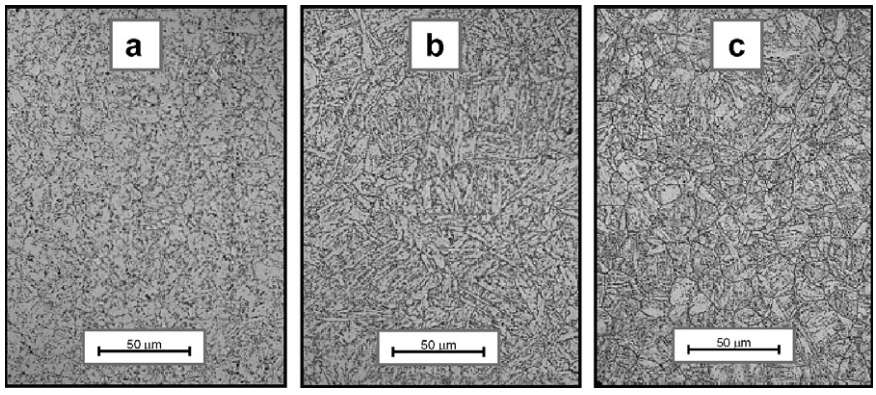

Fig. 1. LOM micrograph of microstructure (a) EUROFER'97, (b) P91 and (c) T91.

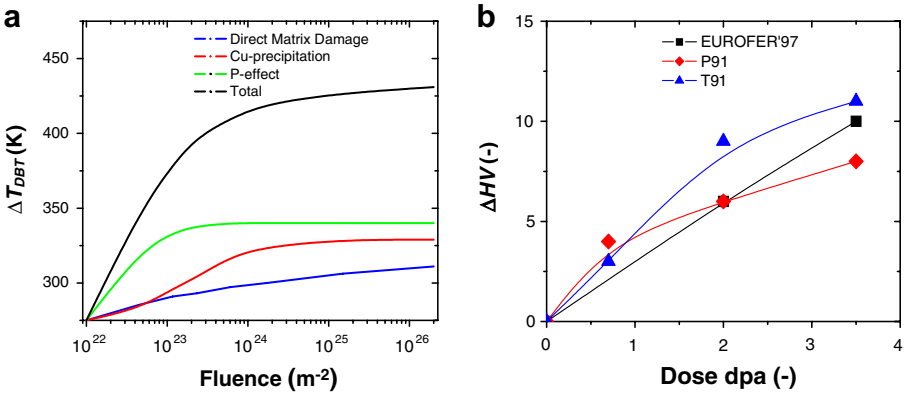

Fig. 2. (a) Model of radiation embrittlement of RPV steels; (b) Hardness parameter versus implantation dose (EUROFER'97, P91 and T91 steel).

there is a general agreement on three sub-processes, which are contributing to radiation damage process: direct matrix damage, copper precipitation and phosphorus segregation (Fig. 2(a)). The key idea for the proton treatment of samples was to simulate the direct matrix damage. Due to this fact, the radiation induced embrittlement caused purely by generation of microstructural effects can be simulated. By plotting the increase of T_{DBT} versus dose, it can be seen that indeed, a power 1/2 function of the dose follows very well the available data, indicating that the shift is related to matrix damage (Fig. 2(a)).

In the case of proton irradiation the damage mechanism can be considered to be a priory dominated by the direct matrix damage. This conclusion can be drawn by the fact that the amount of copper and phosphorus are rather low and nickel is known to enhance matrix damage. Material damage due to direct matrix damage, expressed as the transition temperature shift (ΔT_{DBT}), is normally described as a power 1/2 of the damage parameter Φ

$$\Delta T_{\mathrm{DBT}} = a \cdot \Phi^{n}. \quad (1)$$

3. Results

3.1. Hardness

Three ferritic–martensitic steels have been investigated in order to study their behaviour after different levels of proton irradiation with the aim to monitor irradiation hardening and embrittlement phenomenon. As expected, a non-proportional function of hardness parameter within nickel content was confirmed. An increase of hardness with dose was observed and this phenomenon is assigned to the irradiation hardening. From these outcomes can be assumed that nickel is stabilizing the matrix at increasing of dose level. The hardness measurements on the different samples are given in Fig. 2(b).

3.2. Microstructure

The normalization and tempering treatment results in tempered martensite (i.e. ferrite) structures in all the materials in as received state. Tempered lath martensite containing dislocations and carbides is the primary structural feature. The TEM of microstructures of investigated steels at low magnification is shown in Fig. 3. The microstructures of all the steels after normalization and tempering have similar dislocation substructures. They consist on sub-grains evolving from original martensite laths and dislocation cell network/walls splitting up the laths and joining sub-grain boundaries, in addition to dislocations lines and clusters/tangles inside sub-grains and cells. The sub-grain and lath boundaries are formed by planar, regular arrangement of dislocations. Dislocation cells boundary networks are less regularly organized. Dislocation line densities within laths, sub-grains and cells varies from place to place, ranging from nearly dislocation-free areas to a dense dislocation arrays of interacting line dislocations and dislocation clusters/tangles. Two populations of carbide particles appear in all the steels. Large, blocky $M_{23}C_6$ particles are the predominant type of carbides, ~100 nm in size, of irregular shape. They precipitate primarily on prior austenite, lath, sub-grain and cell boundaries and less frequently also with dislocations within a matrix in all the steels. Several particles were identified

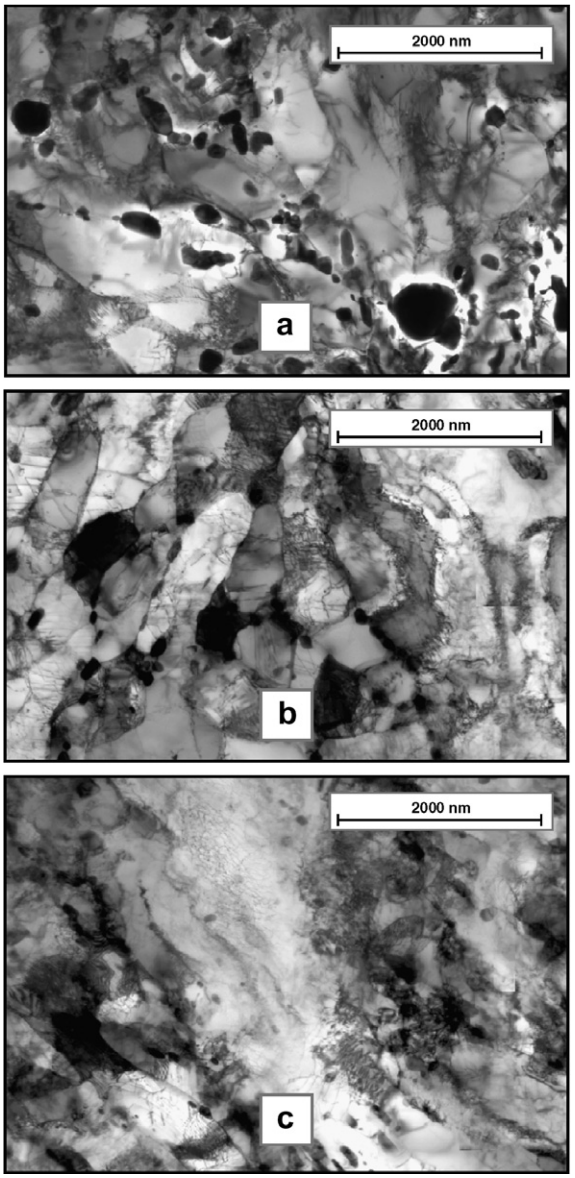

Fig. 3. TEM low magnification composite micrograph: (a) EUROFER'97 steel sub-grain microstructure with $M_{23}C_6$ particles at sub-grains, prior-austenite; (b) P91 steel sub-grains aligned in the direction of original martensite laths, dislocation cell formation (left) boundary (left), agglomeration of carbides (right bottom); (c) T91 steel sub-grain alignment, dislocation cell formation (left), dense dislocation array (middle top).

using selected area diffraction. Small, globular or disc-shaped particles of minor alloying elements with high affinity to carbon precipitate mainly at dislocations within the sub-grain.

EUROFER'97 steel – tempered martensite laths and aligned sub-grains with boundaries decorated by $M_{23}C_6$ particles are typical microstructural features for this steel. The lath width is in the range from 0.1 to 0.25 μm, sub-grains and cells size lies within 0.05–0.1 μm. Dislocation within sub-grains and cells consists of lines or make simple tangles. Total surface dislocation density amounts to $(2.2 \pm 0.7) \times 10^{14}$ m^2. This value seems to be rather high in comparison to 9Cr1MoVNb steels (see below); it may be the result of the fact that higher portion of dislocations (densely spaced) in boundaries has been taken into account. The $M_{23}C_6$ particles, ~200 nm in size, precipitate at boundaries and interact with dislocations in the matrix. Some large particles are constituted by several smaller ones arisen along boundaries. Agglomerates of particles, appear in places, where greater amounts of fine cells occur. Few particles as big as ~1 μm were observed too (Fig. 4). Besides these large, blocky carbides, the smaller, mostly globular, ~0.2 μm in size particles appeared located mainly inside sub-grains. Their density is considerably lower than chromium rich carbides. They probably coincide with (Ta, V)C carbides identified in [14].

P91 steel – the complex, martensite laths and sub-grain microstructure is similar to other ferritic–martensitic steels (Fig. 2). In comparison to EUROFER'97 steel, the lower degree of dislocation recovery and less abundant precipitation is characteristic for this steel. The dislocation density varies from place to place; dense dislocation arrays appear quite frequently. Total surface dislocation density is $(2.7 \pm 0.5) \times 10^{14}$ m^{-2}. The dislocation loops creating in interactions among dislocations moving during tempering appear within dislocations inside sub-grains (Fig. 5(a)). The $M_{23}C_6$ chromium rich carbides, <0.2 μm in size, precipitate mainly along prior austenite grain boundaries and martensite lath boundaries. Particles are slightly smaller and less frequent as in EUROFER'97. In addition to large chromium rich carbides, the small, globular or disc-shaped particles appeared accompanied with boundaries and dislocations inside sub-grains (Fig. 5(b)).

T91 steel – the typical martensitic lath microstructure is very similar to P91 steel (Fig. 2). The total surface dislocation density amounting to $(3.0 \pm 1.3) \times 10^{14}$ m^{-2} is still higher in agreement with lower recovery due to shorter tempering time (Table 1). Standard deviation is higher in this case as dislocation density distribution is considerably heterogeneous in this steel. The population of chromium rich carbides is still less frequent of all the

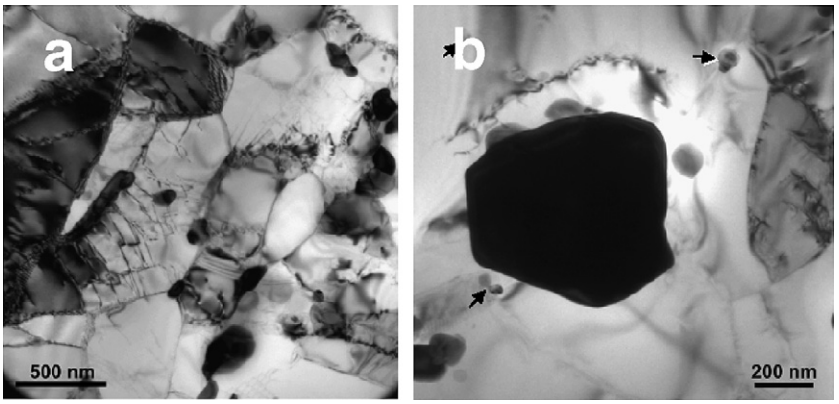

Fig. 4. TEM micrograph of EUROFER'97 steel: (a) sub-grain structure and dislocations; (b) large blocky $M_{23}C_6$ and small globular MC particles.

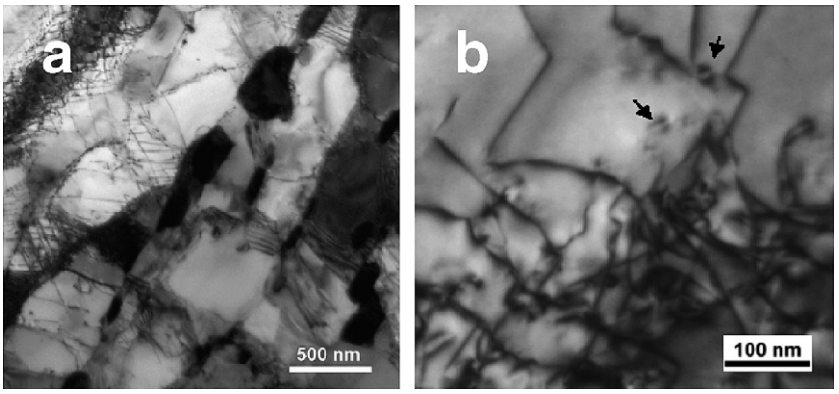

Fig. 5. TEM micrograph of P91 steel: (a) sub-grain formation; (b) dislocation loop (arrowed) formation due to dislocation interactions, cluster/tangles of dislocations (bottom).

steels, especially in less recovered areas (Fig. 6(a)). In addition to large chromium rich carbides, <0.2 μm in size, the small, globular or disc-shaped particles, ~0.1 μm in size, appeared accompanied with boundaries and dislocations inside sub-grains (Fig. 6(b)). No identification of these particles has been done; particles probably correspond to carbides of alloying elements with high affinity to carbon, like vanadium, molybdenum or titanium.

3.3. Positron annihilation

Generally, 2-components and MLT (mean lifetime) analysis for all measured spectra have been applied. The MLT parameter of non-irradiated samples is at a level of 140–145 ps and this value corresponds to the high-alloyed steels (10 wt%). For all studied ferritic–martensitic steels, the MLT parameter is changing very slightly with implantation level and the maximal obtained shift, ΔMLT, is +7 ps. However, 2-components analysis observed a more significant differentiation. Lifetime τ_1 of about 125–135 ps is the dominant high-alloyed steel component with an intensity I_1 of about 70–80%. This component is assigned to the bulk properties and slightly influenced by small carbides of alloying elements with lifetime 100–120 ps (Table 2). The second component τ_2 with intensity $I_2 < 20$–25% and value of about 170–180 ps is assigned to the dislocation loops mainly. However, with increasing of implantation level (dpa) the microstructure has been affected more due to formation of high quantity of vacancy type of defects.

The increase of τ_2 parameter was detected with dose implantation level for all samples (EUROFER'97, P91 and T91). The kinetics of lifetime parameter τ_2 with proton implantation does and hardness is plotted in Fig. 7(a).

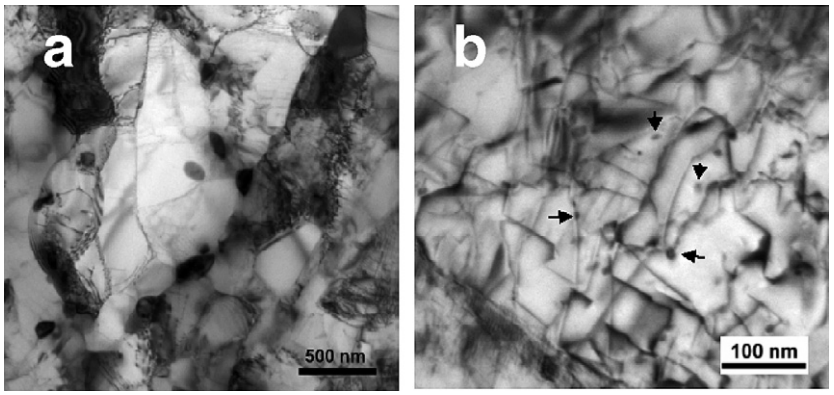

Fig. 6. TEM micrograph of T91 steel: (a) dislocation sub-grains with $M_{23}C_6$ carbides at boundaries and within matrix; (b) evolution of dislocation network within sub-grains, small carbide particles at dislocations (arrowed).

Table 2
Overview of lifetime parameters for various defects and formation of steels

Material	τ (ps)
Fe-bulk [15]	110
Fe-dislocations [16]	165
v_1 (Fe-monovacancy) [15]	175
v_2 (Fe-divacancy) [16]	197
v_3 (Fe-3 vacancy cluster) [16]	232
v_4 (Fe-4 vacancy cluster) [16]	262
VC [17]	99
$V_{0.86}Cr_{0.09}Mo_{0.04}Fe_{0.01}C$ [17]	105
Mo_2C [17]	112
$Mo_{1.4}Cr_{0.6}C$ [17]	116
Cr_7C_8 [17]	107
$Cr_{23}C_6$ [17]	112
$Mn_{26}C_6$ [17]	99
Fe_3C [17]	101

To be mentioned is the fact that by irradiation P91 resulted much more sensitive to radiation than T91 (almost the double shift of τ_2 parameter was obtained, Fig. 7(a)). From the results can be concluded that irradiation causes mainly creation of point defects also enabling their mobility in the material. This outcome indicate that solute-related damage mainly includes direct matrix damage, which is vacancy related. The increase of τ_2 parameter with implantation level (dpa) and hardness of EUROFER'97 has very similar trend-line as for T91 (Fig. 7(b)). These results are very unique and interesting, however more wide studies need to be done, in particular comparison of results with neutron irradiated samples within the aim of quantifying the additional mechanisms of radiation damage and their contributions.

4. Conclusion

The various ferritic–martensitic steels specimens have been studied by application of positron

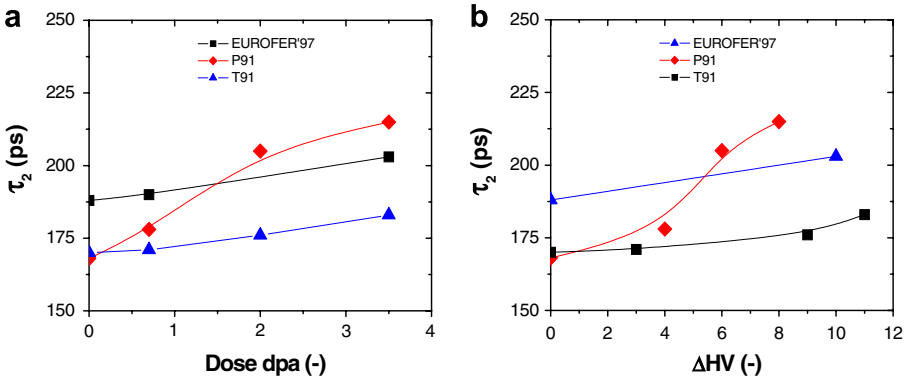

Fig. 7. Kinetics of lifetime parameter τ_2 with (a) proton implantation dose and (b) hardness parameter HV.

annihilation and transmission electron microscopy. Samples of EUROFER'97, P91 and T91 were irradiated by protons to different dpa values and measured and results have been correlated with hardness parameter (HV) and with data from PAS and TEM.

The microstructure of all investigated steel prior proton irradiation is characteristic for tempered martensitic–ferritic steels. The TEM results confirms the decoration of sub-grain boundaries by particles as well as precipitation of carbide particles with dislocations inside sub-grains and this give evidence of interaction between particles and sub-grains and dislocations, resulting in stabilization of the sub-grain structure. Tempered laths and sub-grains with dislocations and carbides are primary microstructural features. Both sub-grain structure and carbide particles evolve during tempering from original lath martensite structure. Sub-grains created by splitting up of laths by dislocation cell network are aligned in the direction of primary martensite laths. Large, blocky chromium rich carbides precipitated mainly at sub-grain boundaries. They are considerably coarser in the EUROFER'97 steel. Small carbides of other carbide-forming alloying elements precipitate at dislocations inside sub-grains. In addition, few large carbide particles precipitate inside sub-grains too. Therefore, P91 has lower radiation stability as T91 and EUROFER'97 respectively. Generally, the degree of tempering-induced recovery of dislocation substructure is significantly higher in the EUROFER'97 steel in comparison to both Fe9Cr1MoVNb steels.

The surface dislocation density of EUROFER'97 ($2.2\times10^{14}\,m^{-2}$), P91 ($2.7\times10^{14}\,m^{-2}$) and T91 ($3\times10^{14}\,m^{-2}$) respectively is changing with the level of dpa dose. Here is an indication based on the analysis of lifetime parameter τ_2 and its intensity I_2 which imply that the concentration of Fe vacancies and divacancies are increasing and the number of dislocations is slightly reduced. However for validation of this hypothesis a complete set of additional TEM measurements of irradiated materials have to be done.

In future, also some other ferritic–martensitic materials could be potentially interested for application in Generation IV concepts, in particular A-21 (9Cr–TiC mod), NF616 (9Cr), HCM12A (12Cr) or 9Cr–2WVTa.

References

[1] G.R. Odette, E.V. Mader, G.E. Lucas, W.S.J. Phythian, C.A. English, in: Proceedings of 16th International Symposium on Effects of Radiation on Materials, ASTM STP 1175, ASTM, 1993, p. 373.
[2] W.J. Phythian, C.A. English, J. Nucl. Mater. 205 (1993) 162.
[3] M. Valo, R. Krause, K. Saarinen, P. Hautojarvi, J.R. Hawthorn, in: Proceedings of 15th International Symposium on Effects of Radiation on Materials, ASTM STP 1125, ASTM, 1992, p. 172.
[4] M.K. Miller, M.G. Burke, J. Nucl. Mater. 195 (1992) 68.
[5] J. Van den Bosch, A. Almazouzi, Reference materials procurement, dispatching and characterization, Report CEN-R-4197, 2005.
[6] A. Zeman, L. Debarberis, V. Slugeň, B. Acosta, Appl. Surf. Sci. 252 (2006) 3290.
[7] V. Slugen, A. Zeman, J. Lipka, L. Debarberis, NDT&E Int. 37 (2004) 651.
[8] J. Cizek, I. Prochazka, J. Kocik, E. Keilova, Phys. Stat. Sol. (a) 178 (2000) 651.
[9] A. Dupasquier, A.P. Mills, Positron Spectroscopy of Solids, IOS, Amsterdam, 1995.
[10] G. Gupta, Z. Jiao, A.N. Ham, J.T. Busby, G.S. Was, J. Nucl. Mater. 351 (2006) 162.
[11] D.S. Gelles, J. Nucl. Mater. 233–237 (1996) 293.
[12] J.J. Kai, R.L. Klueh, J. Nucl. Mater. 230 (1996) 116.
[13] J.F. Ziegler, Nucl. Instrum. and Meth. B 219&220 (2004) 1027.
[14] P. Fernández, A.M. Lancha, J. Lapeña, M. Serrano, M. Hernández-Mayoral, J. Nucl. Mater. 495 (2002) 307.
[15] P. Hautojäarvi, L. Pöllönen, A. Vehanen, J. Yli-Kauppila, J. Nucl. Mater. 114 (1983) 250.
[16] A. Vehanen, P. Hautojäarvi, J. Johansson, J. Yli-Kauppila, P. Moser, Phys. Rev. B 25 (1982) 762.
[17] G. Brauer, M. Sob, J. Kocik, Report ZfK-647, 1990.